Journal of Materials Chemistry C

Microscale screen printing of large-area arrays of microparticles for the fabrication of photonic structures and for optical sorting

Journal:	*Journal of Materials Chemistry C*
Manuscript ID	TC-ART-06-2018-002978.R1
Article Type:	Paper
Date Submitted by the Author:	18-Jul-2018
Complete List of Authors:	Rose, Mark; University of Nebraska - Lincoln, Chemistry Vinod, TP; University of Nebraska - Lincoln, Chemistry; CHRIST (Deemed to be University), Chemistry Morin, Stephen; University of Nebraska - Lincoln, Chemistry; Nebraska Center for Materials and Nanoscience

Journal Name

ARTICLE

Microscale screen printing of large-area arrays of microparticles for the fabrication of photonic structures and for optical sorting

Received 00th January 20xx,
Accepted 00th January 20xx

DOI: 10.1039/x0xx00000x

www.rsc.org/

Mark A. Rose, [†,a] T. P. Vinod,[†,a,c] and Stephen A. Morin*[ab]

There are a limited number of methods applicable to the large-scale fabrication of arrays of discrete microparticles; however, such methods can be applied to the fabrication of structures applicable to photonics, barcoding, and optoelectronics. This manuscript describes a universal method, "microparticle screen printing" (μSP), for the rational patterning of micron-scale particles onto a variety of 2D substrates with diverse mechanical and chemical properties. Specifically, an array of microparticles of different sizes and compositions were patterned onto an array of materials of varying chemistry and stiffness using μSP yielding a diversity of homo/heterogeneous microparticle-based structures. Further, this manuscript reports how the Young's moduli of the substrate can be used to calculate contact area and thus interaction energies (quantified using Hamaker constants) between the particle/substrate during μSP. Generally, μSP is most effective for substrates with low Young's moduli and large Hamaker constants (A_{132}) with the target particles, as confirmed by the performance (quantified using yield and accuracy metrics) of μSP for the different empirically investigated particle/substrate combinations. These understandings allow for the design of optimal surface/particle pairing for μSP and were applied to the fabrication of a diversity of heterogeneous structures, including those with periodic vacancies in HCP (hexagonally closed packed) 2D photonic crystal useful to structural optics, optical particle screening useful to chemical assays, and the fabrication of structural barcodes useful to labeling and anticounterfeiting.

Introduction

The large-scale organization of functional microparticles on various substrates in arbitrary patterns enables applications in a variety of areas, including photonics,[1–3] optoelectronic sensing,[4] biological and chemical assays,[5–8] and labels for anti-counterfeiting.[9,10] Current methods for the preparation of microparticle arrays (e.g., those that use electrostatic interactions,[11,12] molecular interactions,[13,14] optical tweezers,[15,16] electric and magnetic fields,[17,18] etc.) are limited in their ability to achieve precision, scalability, and versatility (in terms of the types of particles and substrates) simultaneously. A general approach applicable to the large-scale assembly of highly ordered arrays of microparticles of various sizes, especially those in the 0-100 μm range, and a diversity of microparticle compositions would be valuable to numerous communities.

In this work, we used flexible polymeric masks comprised of patterned openings to direct the deposition of microparticles onto various surfaces. We prepared masks of various designs using micromolding in capillaries (MIMIC)[19] and deposited microparticles onto substrates through the holes of these masks via the application of mild mechanical pressure. This process has intuitive similarities to the technique of screen printing and we call it "microparticle screen printing" (μSP). The versatility we demonstrated, in terms of the applicability to different classes of substrates (soft and hard substrates) and sizes of particles, was not achievable following existing methods. Additionally, we developed a detailed understanding of how the chemistry and mechanical properties of the particles and substrate influenced the effectiveness of μSP, which could be applied to creating structures that combine different materials beyond those explored herein.

Specifically, the results we describe show the ability of μSP to process large-scale arrays with control over: (i) the relative spatial organization of the microparticles, (ii) the material composition of the substrates and particles, and (iii) the particle sizes deposited in each step of μSP. We utilized these capabilities to fabricate 2D microparticle arrays with simple and sophisticated geometries of various packing schemes, hierarchical assemblies, and monolithic structures with applications in photonics and optical sorting/barcoding useful to sensing, analytical assays, and anticounterfeiting.

The ability to precisely pattern particles has been extensively explored. Generally, these methods, which include the use of optical tweezers,[15,20] optoelectronic tweezers,[21]

[a] Dept. of Chemistry, University of Nebraska-Lincoln, Hamilton Hall, Lincoln, NE 68588, United States.
[b] Nebraska Center for Materials and Nanoscience, University of Nebraska-Lincoln, Lincoln, NE 68588, United States.
[c] Department of Chemistry, CHRIST (Deemed to be University), Hosur Road, Bengaluru 560029, India.
† Mark A. Rose and T.P. Vinod have contributed equally to this work.
Electronic Supplementary Information (ESI) available: Materials and methods, discussion of circle packing and interaction energies. DOI: 10.1039/x0xx00000x

magnetic attraction,[17] coulombic forces,[22,23] hydrophobic-hydrophilic interactions,[24] and acoustic fields,[25] rely on chemical or physical driving forces to generate the target arrays. Despite the diversity of methods, they can be limited in the geometric patterns accessible, the particle sizes and array sizes possible (due to scaling laws of the various interactions), and the specific materials available. They can also be relatively challenging due to the requirement of specialized equipment and expertise in many cases.

Techniques that overcome these limitations through the adoption of scalable methods based on templating, stamping, and printing would be beneficial. Recently, porous microwells were used as templates for obtaining large-scale microgels arrays in a procedure involving microfluidics and pneumatics.[26] We have recently reported a method for the assembly of polymer microstructures that made use of the mechanical deformations of elastic substrates and the surface chemistry of the materials.[27] Herein, we apply this expertise to the development of a strategy, μSP, which adapts the concepts of screen printing to the fabrication of monomeric or polymeric microparticle arrays and assemblies of microparticles.

Experimental Design

Our strategy generally involves the deposition of particles through predefined arrays of holes in flexible masks (Fig. 1a). We chose to use MIMIC as the method to create masks because of the diverse range of pattern designs with micrometer scale dimensions that may be obtained through this approach.[19] Also, the mechanical flexibility of the polymeric materials (e.g., polyurethane, poly(methyl acrylate) (PMA), poly(methyl methacrylate) (PMMA), etc.) compatible with MIMIC allowed the fabrication of templates capable of conformal contact to substrates. We chose substrates (polydimethylsiloxane (PDMS), Ecoflex, silicon, glass, thermoplastic polyurethane (TPU), Parafilm, polyethylene terephthalate (PET), and polycarbonate (PC)) that represent different classes of materials with varying chemical and mechanical properties (Fig. 1 and ESI† text). We used polystyrene microparticles (2 – 30 μm diameter), Fe_3O_4 nanoparticles (34 - 44 nm), glass microparticles (9 – 13 μm diameter), amorphous silica gel (200 – 425 mesh), and amorphous sand (13-25 μm) to illustrate the applicability of this method to different classes of materials with both well or poorly defined geometries and particle size distributions. The physical properties of materials investigated in this study can be found in Table S1. We intentionally focused on commercially available particles and substrates to demonstrate the generality of this method to non-specialized, commodity materials of various functionalities.

Results and Discussion

We successfully deposited particles onto substrates using μSP fabricating specific arrays with the desired order and periodicity (Fig. 1a). We focused our investigations on micron-sized polystyrene (PS) spheres to demonstrate the capabilities of our method, but we were not limited by the chemistry, size (nanometer to micrometer), or mechanical stiffness of PS particles (Fig. S1 and S2, ESI†); however, as we will discuss, the efficiency of μSP was highly dependent on the specific chemical and mechanical properties of the substrate/particle combinations. Specifically, we evaluated the performance of μSP of PS spheres on substrates of varying surface chemistry and surface mechanics including PDMS, Ecoflex, glass, silicon wafers, PET, PC, TPU, and parafilm (Fig. 1b-i). We used quantitative measures to evaluate of the applicability of this technique to each of the substrates using the metrics of 'yield,' 'accuracy,' and 'efficiency' (equations 1 – 3),

$$\textbf{Yield} = \frac{N_o}{N_T} * 100\% \quad \text{Eqn 1}$$

$$\textbf{Accuracy} = \frac{A_{DA}}{A_T} * 100\% \quad \text{Eqn 2}$$

$$\textbf{Efficiency} = \frac{A_{DA}}{A_M} * 100\% \quad \text{Eqn 3}$$

where N_o is number of sites occupied, N_t is the total number of sites, A_{DA} is the area of particles inside designated site, A_T is the total area of the particles patterned, and A_M is the maximum area of particles that can be patterned. Spherical PS

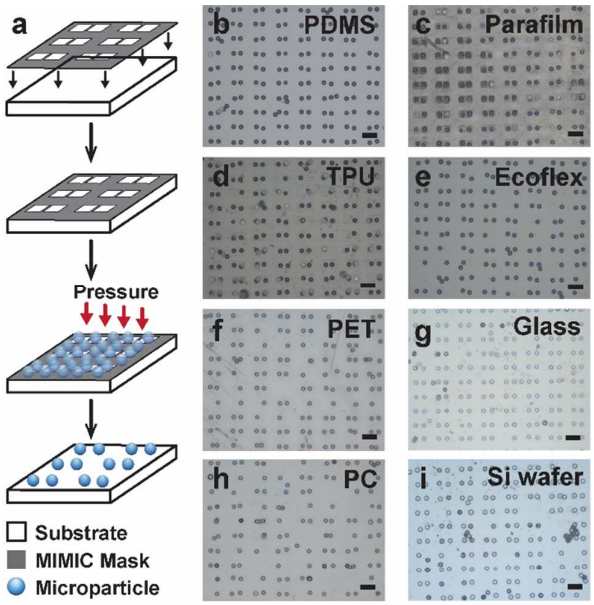

	Yield	Accuracy	Efficiency
PDMS	98 %	89 %	96 %
Parafilm	99 %	84 %	92 %
TPU	94 %	86 %	89 %
Ecoflex	87 %	87 %	86 %
PET	83 %	89 %	80 %
Glass	96 %	73 %	79 %
PC	73 %	93 %	71 %
Si Wafer	86 %	64 %	70 %

Figure 1. (a) Schematic illustration of the microparticle screen printing (μSP) process. (b-i) Optical microscope images of PS microparticle assemblies. The table provides the yield, accuracy, and efficiency of each of the surfaces studied (N = 160 designated sites). All scale bars are 100 μm.

microparticles (30 µm diameter) and a dimer MIMIC pattern (40x40 µm square holes with gaps of 10 µm and 60 µm) were used in these systematic investigations for each substrate. We utilized the 'efficiency' metric to determine the effectiveness of patterning on each surface (ESI† text). We found that PDMS was the preferred surface for the deposition while silicon wafers was the least preferred surface for deposition (Fig. 1). Additionally, we investigated the effect of particle size on the performance of µSP (Fig. S2). We found that, generally, as the particle diameter was decreased, relative to the diameter of the hole in the MIMIC mask, efficiency also decreased, most likely due to higher probabilities of packing defects (Fig. S2 and S3). These results illustrated the general applicability of this process to substrates of varying chemical composition and mechanical properties, but we now moved on to explain the differences in printing efficiency.

We first calculated interaction energies (E_{132}) from Hamaker constants (A_{132}) in order to try and explain why patterning was more effective on certain substrates and less on others (equation 4 and Table S1, ESI†).

$$\mathbf{E_{132}} = \frac{-\mathbf{A_{132}R}}{\mathbf{6*D}} \qquad \text{Eqn 4}$$

Equation 4 defines the interaction of a sphere with a flat surface consisting of two different surfaces (1 and 2) across a medium (3) where E_{132} is the interaction energy (J), A_{132} is the Hamaker constant (J), R is the radius of the sphere (m), and D is the equilibrium distance between two materials (~0.2 nm).[28] We found most Hamaker constants for individual surfaces (A_{11}) in the literature, but values for all the surfaces were not available.[28, 29] In these cases, we related the surface energy (γ) of a substrate to its Hamaker constant (ESI† text) which is generally a good approximation if the surface is non-polar and non-hydrogen bonding.[28] We found that the calculated interaction energies were in disagreement with the trend we observed in the experimental results. They indicated that the silicon-PS interaction energy was the strongest and the PDMS-PS interaction energy was the weakest, but printing was actually most efficient on PDMS (Table S2, ESI†).

To reconcile this disagreement, we considered that our experimental system utilized spherical PS particles and surfaces of differing stiffness that will respond differently to the application of pressure in the printing process. It was clear that calculating interaction energy based on the idealized picture of a sphere on a flat, non-compliant surface was not a comprehensive representation of the experimental conditions used. We thus considered the mechanical properties of the substrates. Specifically, Young's modulus, which can be used in JKR (Johnson-Kendall-Roberts) theory to calculate a contact radius under zero load (equation 5),[28,30]

$$\mathbf{a_0} = \left(\frac{\mathbf{6\pi R^2 E}}{\mathbf{K}}\right)^{\frac{1}{3}} \qquad \text{Eqn 5}$$

where a_0 is the contact radius, R is the radius of the sphere, E is the interaction energy per unit area (ESI† text), and K is the elastic modulus, was used to revaluate the influence of deformation. In particular, we used the contact radius from JKR theory to find the contact area of each particle, and then we calculated the true interaction energies (E_{132}) for the different particle/substrate combinations, where the more negative interaction energies indicate stronger adhesion (Table S3, ESI†). After we made these calculations, we observed that virtually all of the interaction energies correlate with printing efficiency on different surfaces, with the notable exception of Ecoflex, which was lower than expected. We attribute this outlier to possible heterogeneities in the stiffness of Ecoflex. We thus concluded that µSP will, generally, be most effective when substrates with low Young's moduli are used with target particles that give high Hamaker constants (A_{132})

We obtained patterns of PS particles in different periodicities and patterns (Fig. 2) through µSP. We could change the particle size and precisely control the number of particles deposited through the mask by manipulating the dimensions of the openings in the mask relative to the size of the particles and the shape of the openings (Fig. 2). We chose the pattern shape and size in order to change the packing symmetry of the spherical particles from hexagonally close packed (HCP) to simple cubic (Fig. 2b, c, h). Furthermore, we

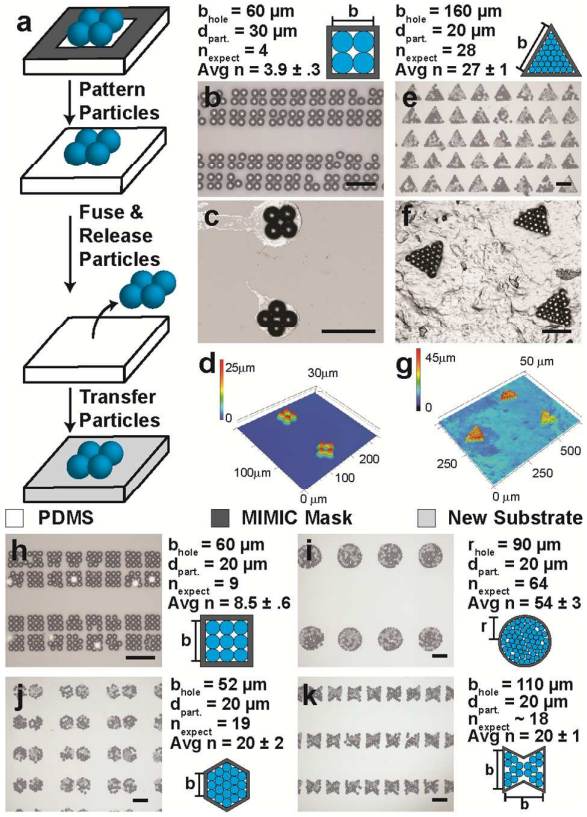

Figure 2. Various microparticle patterns. (a) Schematic illustration of the creation of monolithic structures using µSP. (b-c) Optical images of printing, release, and transfer of PS particles of diameter 30 µm deposited through a mask consisting of square openings with side lengths of 60 µm; (d) Confocal image of the released microstructure consisting of four 30 µm PS spheres. (e-f) Optical images of printing, release, and transfer PS particles of diameter 20 µm deposited through a mask consisting of equilateral triangles openings with 130 µm sides. (g) Confocal image of the released 20 µm PS triangle pattern. (h-k) PS particles of diameter 20 µm printed through masks of different shapes and dimensions. All scale bars are 100 µm and N = 36 designated sites.

could "bond" the particle assemblies through solvent-vapor annealing and we could release the assembled structures as single structural units using water soluble tape (Fig. 2a, c, d, f, g). The ability to bond, release, and transfer the microparticle assemblies to different substrates could be useful to applications where unique polymer microstructures are desired (e.g., high throughput binding assays [4, 31]).

We analyzed the efficiency of μSP of different shapes by comparing the expected number of particles (calculated using equations for the packing of circles into holes of various shapes) to the actual number of particles in each hole (Fig. 2b-k and ESI† text). We found that the various patterns were filled, within experimental error, with the expected number of particles (Fig. 2b, e, h, i, j, k), except in the case of arrays of large circles (Fig. 2i) and 'bowties' (Fig. 2k). We believe that the expected number of particles inside the bowtie pattern may be lower than that observed because this estimate was calculated by fitting the 'bowtie' with 6 triangles (there was no equation for calculating packing in a bowtie directly). In the case of the arrays of large circles (180 μm diameter relative to 20 μm diameter of the particles), we believe that the discrepancy between the expected number of particles and that observed was due to an increase in the number of possible packing defects that are possible for large holes (indeed these defects are readily visible, Fig. S3). Another way of quantifying such packing effects was to calculate the ratio of filled holes (based on ideal packing) to total available holes. For example, when a MIMIC mask with 60 μm square holes was used with 30 μm and 20 μm particles, the ratio of filled to available holes was 86% and 58%, respectively. As ideal packing of 20 μm particles would require a total of 9 particles (versus 4 for 30 μm particles), packing defects are more likely and the calculated ratio was correspondingly smaller. This observation was consistent with studies of particles with variable diameter (Fig. S2). We also acknowledge that, due to shear stress during the application of pressure, the edges of the masks can lose conformal contact with substrate, potentially leading to higher numbers of particles per hole than expected (the comparatively high Young's modulus, 3.0 GPa, of the mask prevents its deformation). We note that in the analysis of the all patterns we only counted the first layer of particles.

We successfully used μSP for the serial deposition of multiple sizes or types of materials onto the same substrate (Fig. 3a-e). We accomplished this by patterning one material followed by patterning of the second type of material, without removing the mask from the substrate after the first step. This procedure illustrates the potential of our method as a strategy for the creation of hybrid materials and assemblies from multiple particle types with different function (e.g., magnetic, optical, etc). Additionally, we could assemble particles of different sizes on different locations within the same pattern through a size selection procedure that was programed by the relative dimensions of the particles and holes in the mask (Fig. 3 f-j). In this case, large particles were deposited first, followed by smaller particles. Such structures could be useful in generating arrays of hierarchical/heterogeneous particle assemblies with applications in, for example, optical waveguides and photonics.[1–3]

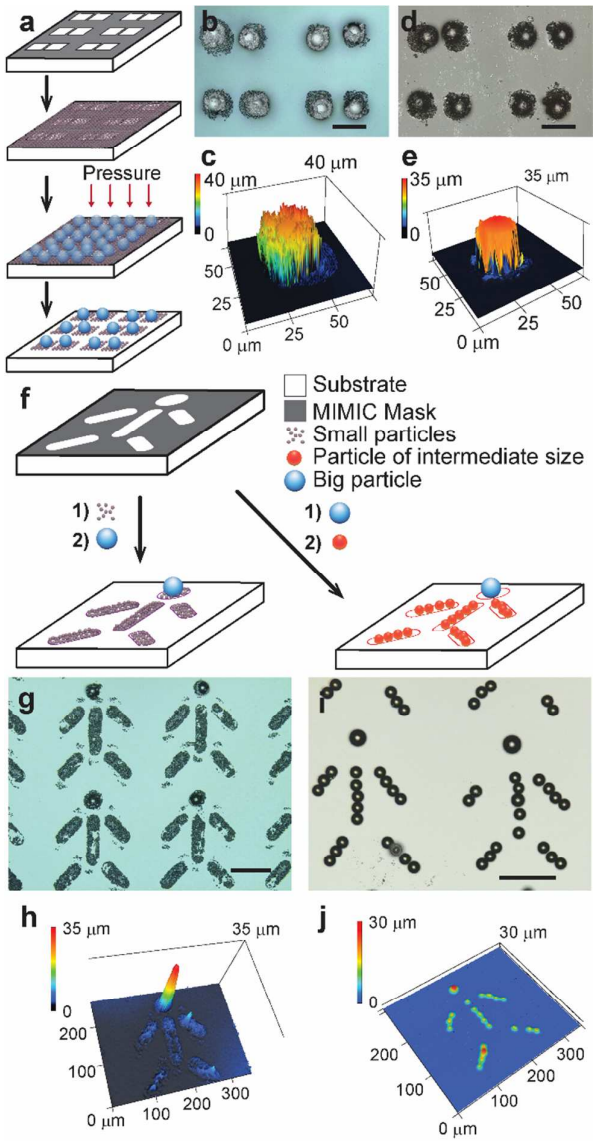

Figure 3. Heterogeneous assembly through serial μSP. (a) Schematic illustration of the process; (b-c) Optical micrograph (b) and confocal topography map (c) of a heterogeneous assembly of two types of PS particles with diameters 2 μm and 30 μm respectively. (d-e) Optical micrograph (d) and confocal topography (e) of a heterogeneous assembly of Fe_3O_4 nanoparticles (34 - 44 nm diameter) and PS particles (30 μm diameter). (f) Schematic of the serial deposition of different size particles. (g-h) Optical micrograph (g) and confocal topography (h) of a stick figure generated using a MIMIC mask with 20 and 30 μm openings filled with 2 and 30 μm particles. (i-j) Optical micrograph (i) and confocal topography map (j) of a stick figure generated using a MIMIC mask with 20 and 30 μm openings filled with 20 and 30 μm particles. Scale bars: 50 μm (for b and d) and 100 μm (for g and i).

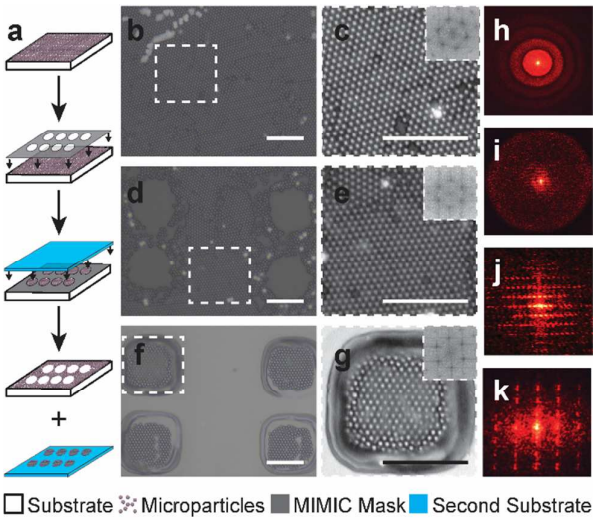

Figure 4. Fabrication of patterned 2D photonic crystals. (a) Schematic illustration of the formation of patterned vacancies in a 2D photonic crystal using µSP. (b) Optical micrograph of a film of hexagonally close packed PS particles (2 µm diameter). (c) Zoomed in optical micrograph of the HCP particles shown in (b). (d) Optical micrograph of the patterned vacancies created by transferring particles to scotch tape through a MIMIC mask with circular openings. (e) Zoomed in optical micrograph of interstitial HCP particles shown in (d). (f) Optical micrograph of particles transferred to the scotch tape. (g) Zoomed in optical micrograph of transferred HCP particles shown in (f). (c, e, g) FFT of the hexagonal closed packed arrays for the corresponding optical images in b-f. (h-j) Far field interference patterns of (d, e) with the substrate at three different distances (0.3, 0.9, and 1.8 m respectively) from the imaging plane. (k) Far field interference pattern from (f, g) at 1m. All scale bars are 25 µm.

We used µSP to remove particles from an HCP 2D photonic crystal to create patterned vacancies in the structure and thus modulate the optical signature of the crystal (Fig. 4a). To achieve this, we first created a HCP array of PS on a PDMS surface (Fig. 4b, c). We then removed particles *through* openings in a MIMIC mask using a transfer substrate (scotch tape), creating patterned vacancies in the photonic crystal (Fig. 4d, e). When we observed the optical performance of the resulting patterned 2D photonic crystal we observed the expected interpenetration of the HCP and square array interference patterns in the far field interference pattern of the 2D photonic crystal (Fig. 4h-j). The particles removed in this procedure constituted a complementary pattern of the vacancies and they were easily transferred onto a new host substrate (Fig. 4f, g) and created far field interference pattern consistent with the ordering of a square array (Fig. 4k). We used optical microscopy and FFT analysis to demonstrate that the original HCP structure was retained throughout the process of removal and transfer (Fig. 4c, e, g insets). The ability to create periodic holes in 2D photonic structures could find application in the structural optics and photonics.[1–3]

Another application, though not initially obvious, was the use of µSP to measure relative concentrations of different sized microparticles in solutions using concepts of particle counting and computer edge finding algorithms. We demonstrated this concept using arrays printed with a mask consisting of equilateral triangular holes (edge length = 160 µm) and PS microparticles of two different sizes (20 µm and 30 µm diameter). Each individual triangular hole can accommodate up to 28 particles that are 20 µm in diameter or 10 particles that are 30 µm in diameter (based on the packing of circles into triangle, see ESI†). Thus, any given mixture of particles was expected to give arrays of triangles with some ideal number of large versus small particles following the µSP process. We made a series of solutions with varying ratios of

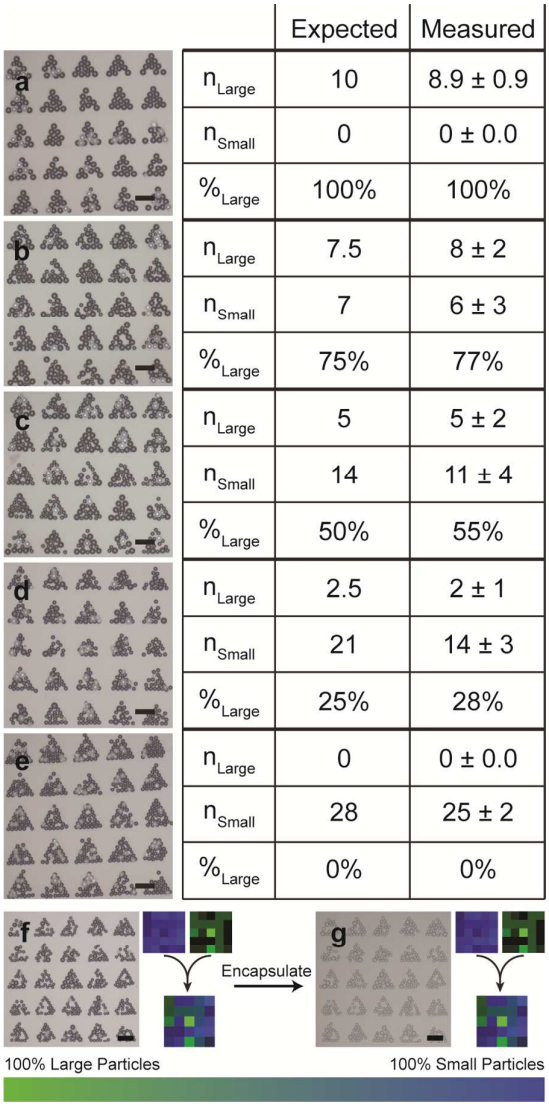

	Expected	Measured
n_{Large}	10	8.9 ± 0.9
n_{Small}	0	0 ± 0.0
$\%_{Large}$	100%	100%
n_{Large}	7.5	8 ± 2
n_{Small}	7	6 ± 3
$\%_{Large}$	75%	77%
n_{Large}	5	5 ± 2
n_{Small}	14	11 ± 4
$\%_{Large}$	50%	55%
n_{Large}	2.5	2 ± 1
n_{Small}	21	14 ± 3
$\%_{Large}$	25%	28%
n_{Large}	0	0 ± 0.0
n_{Small}	28	25 ± 2
$\%_{Large}$	0%	0%

Figure 5. Microparticle sorting using µSP. (a-e) Optical images of 25 well arrays patterned with different concentrations of 20 and 30 µm PS particles. The corresponding table shows the expected number of particles per hole, the calculated number of particle found using an edge finding algorithm (confirmed by manual counting) and the volume percent of large particles in the solution. f) Optical image and pixel representations of the PS microparticles of 20 µm and 30 µm diameter deposited on PDMS surface through a MIMIC mask. The blue pixel diagram was generated using the number of 20 µm particles. The green pixel diagram was generated using the number of 30 µm particles. The final pixel diagram is an overlay obtained by merging of the blue and green diagrams. (g) Optical image and pixel diagrams generated from the same pattern as (f) encapsulated in a PDMS layer. All scale bars are 100 µm.

large: small particles and used them to create triangular arrays following the μSP procedure. We then used edge-finding algorithms (and manual counting) to evaluate a 5×5 array of triangles for each of the stock mixtures, measuring the average number and ratio of large to small particles in each case. Following this procedure, the measured percent agreed with that expected packing within 5% (Fig 5 a-e). We believe that this simple method for determining the concentration of two different sized particles could be useful in analytical assays, forensics analysis, and the separation sciences.

As reflected by the standard deviations in the measured particle populations across the 5×5 arrays (Fig. 5), there can be a deviation in the ratio of large to small particles for different triangles. This characteristic of heterogeneous μSP presents the opportunity to make, automatically, populations of unique structures that can behave as bar-code-like markers for discrete labelling applications (Fig. 5f, g). For example, when and analogous 5x5 array of 160 μm sided equilateral triangles is patterned with two different sizes of polystyrene (20 μm and 30 μm diameter) microparticles there exist 10^{61} possibilities (280 possible combinations of 20 μm particles and 30 μm particles in a single triangle with 25 total triangles across the array) for the packing of the spheres in the array. Since there is little control over how the spheres ultimately pack, there is an infinitesimal probability that the same array will be duplicated in another deposition and replicating the array using other techniques would be difficult. These characteristics make this method appealing for the fabrication of bar-code-like markers—they are unique, easy to produce randomly, and hard to replicate. Further, it was easy to encapsulate the particle arrays in different polymers (e.g., PDMS), without disturbing the array, for transfer to other surfaces or a wash step (Fig. S4). An overlay of the three optical micrographs illustrates this capability (Fig. S4e). Furthermore, we developed an optical coding system that made it easy to visualize the heterogeneities within individual triangles and across different arrays. This procedure involved assigning a B and G (from the RGB color scheme) that was proportional to the number of small and large particles, respectively (Fig. 5f, g). By summing these individual channels into a pixel array, visualizing the "barcode" in color format was straight forward and it collapsed large image files into smaller data formats. These microparticle based "barcodes" could be useful to optical encoding for application in anti-counterfeiting and randomly generated labelling technologies.[32]

Conclusions

In this study, we presented a method, μSP, for the deterministic assembly of microparticles on solid surfaces. Masks prepared through MIMIC were used to guide and control the periodicity and symmetry of particle assemblies. We fabricated assemblies of various microparticles on a range of substrates with varying chemical composition and physical features. This is the first example of a straightforward templating procedure used to obtain large-scale arrays of pre-synthesized particles in geometries with limited constraints. We demonstrated the potential of our method to obtain monolithic structures comprising of precisely controlled number of components, heterogeneous assemblies, patterned 2D photonic crystals, and assemblies that can used as unique "bar-code-like" structures. We also demonstrated how the surface chemistry and surface mechanics affect the efficiency of μSP. The main advantage of this procedure is that the process is intuitive in nature and allows the patterning of a large number of particles onto a variety of surfaces over large areas. The method is also not destructive to the mask meaning a single mask can be reused in multiple μSP processes which helps alleviate deviation from sample to sample. When using μSP it is important to consider the surfaces properties of the substrates and particles in order to optimize printing efficiency. Doing so appropriately will enable the use of μSP with greater varieties of materials of diverse functional properties beyond those investigated here (Table S1). The approach presented in this study could be useful to a number of fields using functional micro/nanostructures in particular structural optics and displays, photonics, biosensing, anti-counterfeiting, and analytical assays.

Conflicts of interest

There are no conflicts to declare.

Acknowledgements

We thank the Department of Chemistry and the Nebraska Center for Materials and Nano Science (NCMN), at the University of Nebraska–Lincoln, and the University of Nebraska–Lincoln for start-up funds. S.A.M. thanks 3M for support through a Non-Tenured Faculty Award. This work was partially supported by the National Science Foundation under Grant No. 1555356. This research was performed in part at the NanoEngineering Research Core Facility, and at the Nebraska Nanoscale Facility: National Nanotechnology Coordinated Infrastructure and the Nebraska Center for Materials and Nanoscience, which are supported by the National Science Foundation under Award ECCS: 1542182, and the Nebraska Research Initiative.

References

1 M. Notomi, K. Yamada, A. Shinya, J. Takahashi, C. Takahashi and I. Yokohama, *Physical Review Letters*, 2001, **87**.
2 T. Ding, S. K. Smoukov and J. J. Baumberg, *Nanoscale*, 2015, **7**, 1857-1863.
3 P. F. Jing, J. D. Wu and L. Y. Lin, *ACS Photonics*, 2014, **1**, 398-402.
4 S. Carregal-Romero, E. Caballero-D'Iaz, L. Beqa, A. M. Abdelmonem, M. Ochs, D. Ähuhn, B. S. Suau, M. Valcarcel and W. J. Parak, *Annu. Rev. Anal. Chem.*, 2013, **6**, 53-81.
5 C. N. LaFratta and D. R. Walt, *Chem. Rev.*, 2008, **108**, 614-637.
6 D. C. Pregibon, M. Toner and P. S. Doyle, *Science*, 2007, **315**, 1393-1396.
7 D. M. Rissin, C. W. Kan, T. G. Campbell, S. C. Howes, D. R. Fournier, L. Song, T. Piech, P. P. Patel, L. Chang, A. J. Rivnak,

E. P. Ferrell, J. D. Randall, G. K. Provuncher, D. R. Walt and D. C. Duffy, *Nat. Biotechnol.*, 2010, **28**, 595-599.
8 S. E. Chung, J. Kim, D. Y. Oh, Y. Song, S. H. Lee, S. Min and S. Kwon, *Nat. Commun.*, 2014, **5**.
9 S. Han, H. J. Bae, J. Kim, S. Shin, S. E. Choi, S. H. Lee, S. Kwon and W. Park, *Adv. Mater.*, 2012, **24**, 5924-5929.
10 H. J. Bae, S. Bae, C. Park, S. Han, J. Kim, L. N. Kim, K. Kim, S. H. Song, W. Park and S. Kwon, *Adv. Mater.*, 2015, **27**, 2083-2089.
11 S. O. Lumsdon, E. W. Kaler, J. P. Williams and O. D. Velev, *Appl. Phys. Lett.*, 2003, **82**, 949-951.
12 M. E. Leunissen, C. G. Christova, A. P. Hynninen, C. P. Royall, A. I. Campbell, A. Imhof, M. Dijkstra, R. Van Roij and A. Van Blaaderen, *Nature*, 2005, **437**, 235-240.
13 T. Kaufmann, M. T. Gokmen, S. Rinnen, H. F. Arlinghaus, F. Du Prez and B. J. Ravoo, *J. Mater. Chem.*, 2012, **22**, 6190-6199.
14 M. Zimmermann, D. John, D. Grigoriev, N. Puretskiy and A. Böker, *Soft Matter*, 2018, **14**, 2301-2309.
15 J. P. Hoogenboom, D. L. J. Vossen, C. Faivre-Moskalenko, M. Dogterom and A. Van Blaaderen, *Appl. Phys. Lett.*, 2002, **80**, 4828-4830.
16 T. Čižmr, L. C. D. Romero, K. Dholakia and D. L. Andrews, *J. Phys. B*, 2010, **43**.
17 S. Tasoglu, C. H. Yu, H. I. Gungordu, S. Guven, T. Vural and U. Demirci, *Nat. Commun.*, 2014, **5**.
18 K. S. Khalil, A. Sagastegui, Y. Li, M. A. Tahir, J. E. S. Socolar, B. J. Wiley and B. B. Yellen, *Nat. Commun.*, 2012, **3**.
19 E. Kim, Y. Xia and G. M. Whitesides, *J. Am. Chem. Soc.*, 1996, **118**, 5722-5731.
20 K. Dholakia, P. Reece and M. Gu, *Chem. Soc. Rev.*, 2008, **37**, 42-55.
21 A. T. Ohta, P. Y. Chiou, T. H. Han, J. C. Liao, U. Bhardwaj, E. R. B. McCabe, F. Yu, R. Sun and M. C. Wu, *J. Microelectromech. Syst.*, 2007, **16**, 491-499.
22 N. V. Dziomkina and G. J. Vancso, *Soft Matter*, 2005, **1**, 265-279.
23 A. Yethiraj and A. Van Blaaderen, *Nature*, 2003, **421**, 513-517.
24 I. Lee, H. Zheng, M. F. Rubner and P. T. Hammond, *Adv. Mater.*, 2002, **14**, 572-577.
25 C. E. Owens, C. W. I. Shields, D. F. Cruz, P. Charbonneau and G. P. López, *Soft Matter*, 2016, **12**, 717-728.
26 J. J. Kim, K. W. Bong, E. Reátegui, D. Irimia and P. S. Doyle, *Nat. Mater.*, 2017, **16**, 139-146.
27 T. P. Vinod, J. M. Taylor, A. Konda and S. A. Morin, *Small*, **2017**, **13**.
28 J. N. Israelachvili, *Intermolecular and Surface Forces, 3rd Edition*, 2011**.**
29 L. Bergstrom, *Adv. Colloid Interface Sci.*, 1997, **70**, 125-169.
30 K. L. Johnson, K. Kendall and A. D. Roberts, *Proc. Royal Soc. A*, 1971, **324**, 301-313.
31 C. J. Flaim, S. Chien and S. N. Bhatia, *Nature Methods*, 2005, **2**, 119-125.
32 J. Lee, P. W. Bisso, R. L. Srinivas, J. J. Kim, A. J. Swiston and P. S. Doyle, *Nat. Mater.*, 2014, **13**, 524-529.

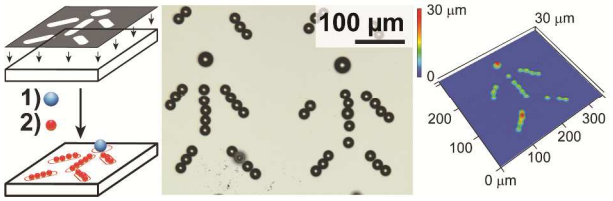

TOC Caption. This report describes a new strategy, microparticle screen printing (µSP), generally applicable to the fabrication of homo/heterogeneous arrays of functional particles with potential applications in photonics, optoelectronics, and optical sorting/barcoding.